

## EXPERIMENTAL AND COMPUTATIONAL SIMULATIONS OF THE FLOWS OVER BACKWARD FACING STEP

Willis Alcantara Manzan Júnior  
 Carlos Alberto de Almeida Vilela  
 Felipe Pamplona Mariano

Universidade Federal de Goiás, Escola de Engenharias Elétrica, Mecânica e de Computação  
 Av. Universitária, 1488, Bloco: A, Piso: 3  
 Setor Leste Universitário  
 CEP: 74605-010, Goiânia, GO.  
 willismanzan@gmail.com  
 carlosavgeo@yahoo.com  
 fpmariano@emc.ufg.br

**Abstract.** To test and validate the numerical codes in Computational Fluid Dynamics (CFD) the comparison with experimental results is very useful, furthermore, the choice of the problem test is important. In the present paper the classical problem in CFD is used: the flow over backward facing step, to validate a numerical method is used, Fourier pseudospectral (FSM) methods. The flow over backward facing step is a complex flow with detachment and reattachment points of boundary layers, to high Reynolds numbers, the Kelvin-Helmholtz instabilities should appear and is possible visualize others flow structures. The experiment procedure consists of smoke and laser visualization in subsonic wind tunnel. The inferior and superior recirculation lengths, for different Reynolds numbers are obtained and compared with the numerical results.

**Keywords:** Flow over backward facing step, Fluid Dynamics, Fourier Pseudospectral Method

### 1. INTRODUCTION

The backward-facing step is one of the most commonly used test cases for verifying the potential of a new methodology and new implementations of numerical codes to CFD. It is geometrically simple and presents a high control of the boundary layer detachment point. On the other hand, it generates a notably complex flow with detachment and reattachment points, shear flow, recirculation zones and boundary layers. Many related experimental reports have been published, for instance Armaly *et al.*, (1983) and Lee and Mateescu (1998), as well as, numerical results, Gartling (1990) and Moin and Kin (1997).

Figure 1 shows the expected physical characteristics of the flow over this geometry. The geometry is characterized by an entrance channel of length,  $L_u$ , and height,  $W-h$ . The step has a height  $h$ . The channel after the step has length  $L_d$  and height  $W$ . The ratio  $W/h$  is known as the aspect ratio.

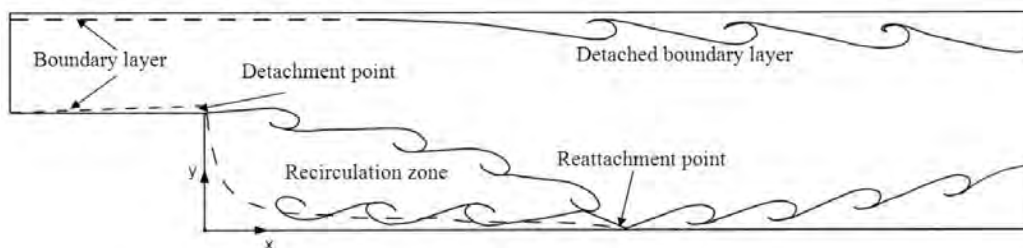


Figure 1. Physical characteristics expected to backward-facing step flows.

Figure 4 illustrates the boundary layers at the inlet channel. The detachment of the boundary layer at the bottom wall occurs at  $(x=0; y=h)$  independently of the flow upwind of this point. The boundary layer reattaches at  $(x=X_1; y=0)$ . The boundary layer at the top wall detaches at  $(x=X_4; y=W)$  and reattaches at  $(x=X_5; y=W)$ . The detachment of the bottom wall boundary layer promotes a recirculation zone and creates a mean inflectional velocity field, which gives rise to Kelvin-Helmholtz instabilities. The adverse pressure gradient downstream of the step causes the top wall boundary layer to detach and creates Kelvin-Helmholtz instabilities below the top wall.

Phenomena involving aeroacoustic, transition to turbulence and combustion are problems that modern engineering aim to understand, among other manners, using techniques of the Computational Fluids Dynamics (CFD). In the case of the aeroacoustic is important to use a method that captures the sound pressure waves. The combustion flows exists processes that involve the small edges of the turbulent flow. In phenomena involving transition to turbulence is necessary to study the small instabilities that become the flows turbulent. In all these problems the CFD uses methods

W.A. Mazan Júnior, C.A.A. Vilela and F.P. Mariano  
 Experimental and Computational Simulations of the Flow over Backward Facing Step

of high order accuracy to obtain results for analyses which represent the physics phenomena aforementioned. The high order methods provide an excellent accuracy, for example: the methods of high order finite differences and the compact schemes, on the other hand, they have as disadvantaged the computational expensive cost in comparison to the conventional methodologies. The advent of the spectral methods joining high accuracy with low computational cost became possible. This low cost is given by the Fast Fourier Transformed (FFT), since the cost of a problem resolution with finite differences is the order of  $O(N^2)$ , where  $N$  is the number of the grid points, the cost of the FFT is of  $O(N \log_2 N)$  (Canuto *et al.*, 1988).

Furthermore, the projection method was also developed (Silveira-Neto, 2002; Souza, 2005), which disentails pressure field of the Navier-Stokes equations in the spectral space. Using the projection process does not need to solve the Poisson equation, like it is given by the conventional methodologies. Normally, solving this equation is the most expensive part of a CFD code. The disadvantage of the spectral methodology is the difficulty to work with complex geometries and boundary conditions.

In the present paper the methodology tested use the Fourier pseudospectral method connected in the immersed boundary method. It is proposed to simulate flows with non-periodic boundary conditions making use of the term source of the immersed boundary method (IBM). The IBM arise to solve computational efficiently flow problems over complex and deformable geometries (Peskin, 2002). The grid in IBM is always regular spaced (Fig. 1b), and the geometry is represented by a source term in Navier-Stokes equations.

The present paper a numerical methods is used to solve the flows over backward-facing step: the IMERSPEC (Mariano *et al.*, 2010) are the combination of Fourier Spectral and Immersed Boundary methods. The results of reattachment and detachment points of flows over backward-facing step are compared which the experiment.

## 2. EXPERIMENTAL VISUALIZATION OF INSTABILITIES

### 2.1 Experimental setup

The experimental setup consists of an open air-driven flow channel (Armaly *et al.*, 1983), which contains two square ducts designed an expansion ratio  $W/h=2$ , that models the backward-facing step (Figure 2 left) coupled with a cooler an outlet duct (Figure 2 right).

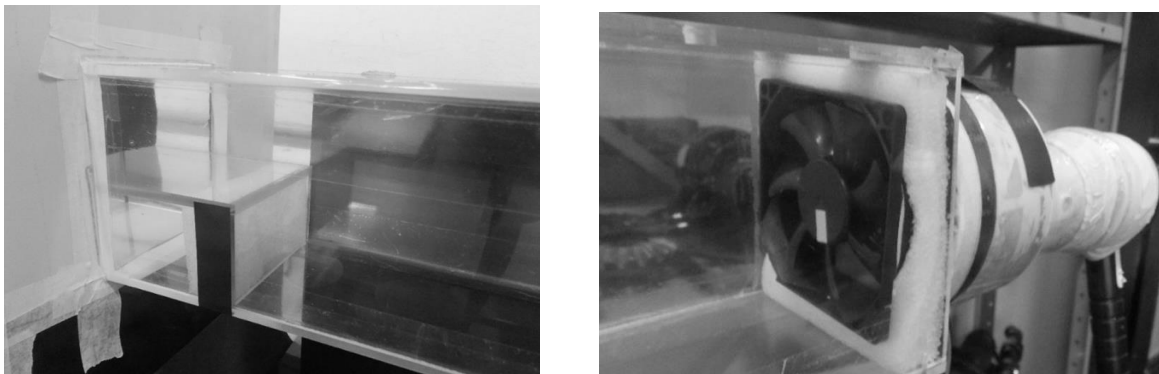


Figure 2. Details of: a) inlet duct: models the backward-facing step, b) outlet duct: cooler and anemometer coupled.

The cooler velocity is controlled by electrical power source and is connected to an anemometer. The power source is adjusted and the anemometer is verified until the mean velocity of the flow given the suitable Reynolds number:

$$\text{Re}_h = \frac{\bar{U}h}{\nu}, \quad (1)$$

where  $h$  is the high of backward-facing step [m],  $\nu$  is the kinematic viscosity coefficient [ $m^2/s$ ] and  $\bar{U}$  is the mean inlet duct velocity [ $m/s$ ].

In order to visualize the flow into the duct a smoke machine and a laser generator are used. The convex lens is placed in front of point laser (Figure 3), such that, the laser point converts in planar laser, by mean of the light diffraction. The light diffraction perform a laser plane, which lighting the specific positions of test section.

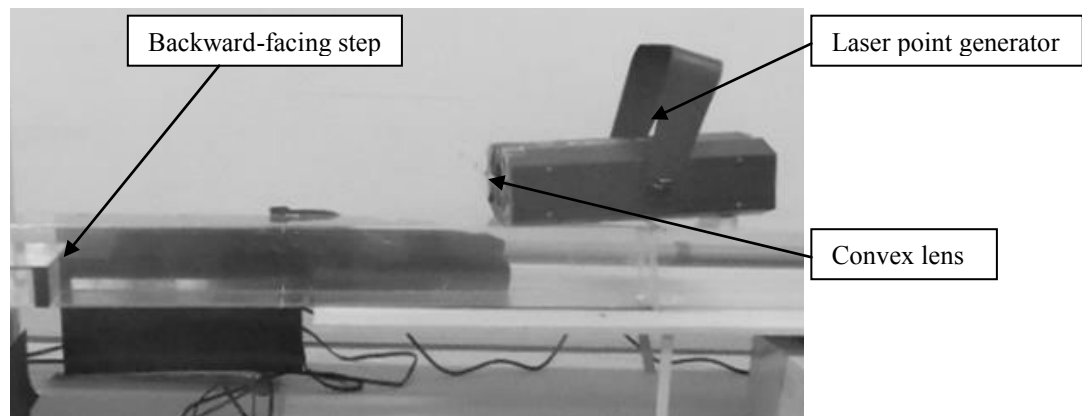


Figure 3. Laser generator placed over section test of wind tunnel.

## 2.2 Experimental results

The sketch of test section is shown in Figure 4 right, where the lengths of test section are:

- High of step:  $h=4.8 \cdot 10^{-2} \text{ m}$ ;
- Inlet duct length:  $L_u=2.0 \cdot 10^{-1} \text{ m}$ ;
- Outlet duct length:  $L_d=1.8 \cdot 10^0 \text{ m}$ .

The variables  $X_1$ ,  $X_4$  and  $X_5$  are the points of inferior reattachment, superiors detachment and reattachment, respectively. In Figure 4 left are shown the snapshot for different Reynolds numbers in symmetrical plane ( $z=h$ ) of backward-facing step section test.

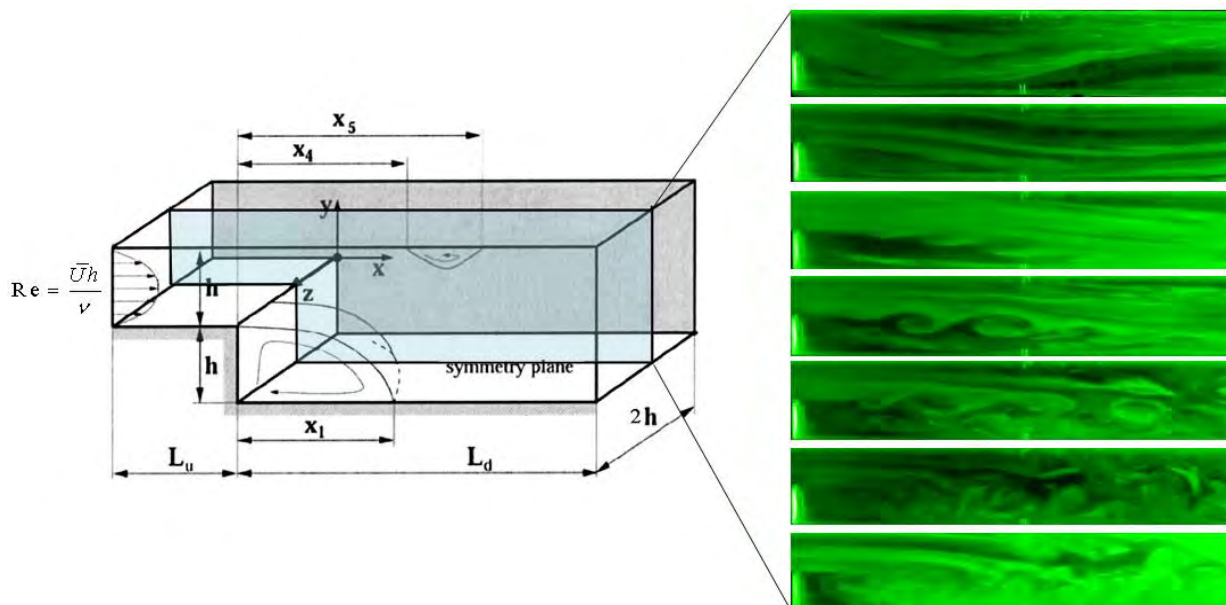


Figure 4. Sketch of test section and snapshot of flows over backward-facing step from  $Re_h=100$ , 500, 1000, 1500, 2000, 2500 and 3000 (from top to bottom).

When the Reynolds number is small ( $Re_h=100$  and 500) two recirculations are formed, one inferior and, the other superior, the laminar and steady flow are observed. The recirculation at  $Re_h=500$  is larger than  $Re_h=100$ , as well as, in Armaly *et al.*, (1983). At the  $Re_h=1000$ , 1500 and 2000, the flows pass to transitional region from laminar to turbulent, The Kelvin-Helmoltz instabilities are generated, at  $Re_h=1500$  is very clear to see this important phenomenon. At  $Re_h=2500$  and 3000 the flow is turbulent and a lot of structures eddies are raised.

Figure 5 presents two pictures obtained at  $Re_h=1000$ . The left picture, in Figure 5, is a snapshot of instant that smoke is released in the channel. Then, the time passes, and the smoke is driven out of the channel. However, the recirculation does not allow that part of air leave the channel. This phenomenon can be observed by smoke that arrest into recirculation zone, by generating a contrast to picture. Furthermore, a second recirculation arises. It is induced by the first one, at corner of step.

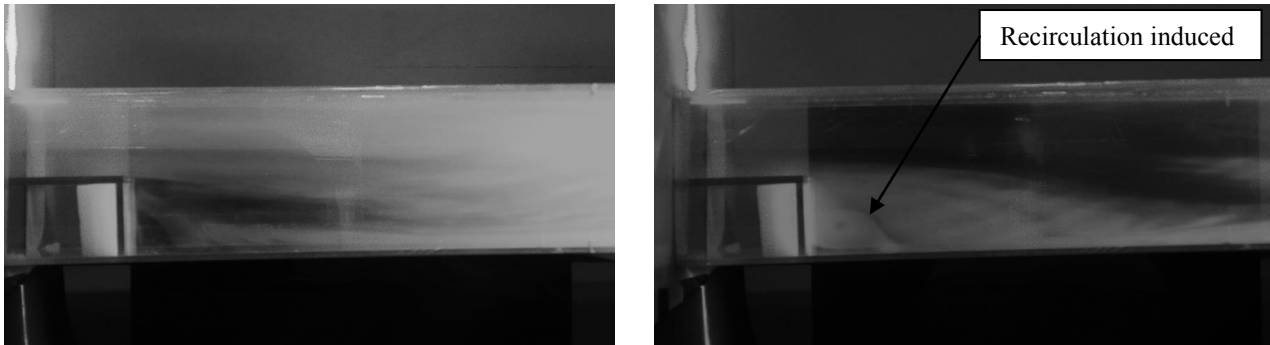


Figure 5. Flow over backward-facing step at  $Re_h=1000$ : picture of smoke is release to channel (left). Picture of the smoke arrest into recirculation zone (right).

### 3. MATHEMATICAL MODELING

In the present section the formulation to two-dimensional Navier-Stokes and continuity equations to incompressible flows are demonstrated

#### 3.1 Mathematical model for the fluid

The flow is modeled by conservation momentum equation (Eq. 2) and the continuity equation (Eq. 3). The equations that model the problem are presented in their tensorial form:

$$\frac{\partial u_i}{\partial t} + \frac{\partial(u_i u_j)}{\partial x_j} = -\frac{\partial p}{\partial x_i} + \nu \frac{\partial^2 u_i}{\partial x_j \partial x_j} + f_i \quad (2)$$

$$\frac{\partial u_j}{\partial x_j} = 0 \quad (3)$$

where  $\frac{\partial p}{\partial x_i} = \frac{1}{\rho} \frac{\partial p^*}{\partial x_i}$ ;  $p^*$  is the static pressure in  $[N/m^2]$ ;  $u_i$  is the velocity in  $i$  direction in  $[m/s]$ ;  $f_i = \frac{f_i^*}{\rho}$ ;  $f_i^*$  is the term source in  $[N/m^3]$ ;  $\rho$  is the density;  $\nu$  is the cinematic viscosity in  $[m^2/s]$ ;  $x_i$  is the spatial component  $(x,y)$  in  $[m]$  and  $t$  is the time in  $[s]$ . The initial condition is any velocity field that satisfies the continuity equation.

#### 3.2 Mathematical model for Immersed Boundary Method

In IBM method the information of the fluid/solid interface (domain  $\Gamma$ ) is passed to the eulerian domain ( $\Omega$ ) using a term source to Navier-Stokes equations. This term plays a role of a body force that represents the boundary conditions of the immersed geometry (Goldstein *et al*, 1993). The source term is defined in all domain  $\Omega$ , but presents different values from zeros only in the points that coincide with the immersed geometry (Eq. 4), enabling that the eulerian field perceives the presence of solid interface (Enriquez-Remigio and Silveira Neto, 2007).

$$f_i(\vec{x}, t) = \begin{cases} F_i(\vec{x}_k, t) & \text{if } \vec{x} = \vec{x}_k \\ 0 & \text{if } \vec{x} \neq \vec{x}_k \end{cases} \quad (4)$$

where  $\vec{x}$  is the position of the particle in the fluid and  $\vec{x}_k$  is the position of a point in solid interface (Fig. 4).

The lagrangian force field is calculated by direct forcing methodology, which was proposed by Uhlmann (2005). One of the characteristics of this model is modeling the non-slip boundary condition on immersed interface.

The Eq. (4) can be conclude that the field  $f_i(\vec{x}, t)$  is discontinuous, which can be numerically solved only when there are coincidence between the points that compose the interface domain and the composes the fluid domain. The Lagrangean force field, in the present study, is calculated by the direct forcing method (DFM), which was proposed by Wang *et al*. (2008). One of the characteristics of this model is that is not necessary to use *ad-hoc* constants and allows the non-slip condition modeling on immersed interface. The Lagrangean force,  $F_i(\vec{x}_k, t)$ , is available by momentum conservation equation over a fluid particle that is joined in the fluid-solid interface:

$$F_l(\vec{x}_k, t) = \frac{\partial u_l}{\partial t}(\vec{x}_k, t) + \frac{\partial}{\partial x_j}(u_l u_j)(\vec{x}_k, t) + \frac{\partial p}{\partial x_l}(\vec{x}_k, t) - \nu \frac{\partial^2 u_l}{\partial x_j \partial x_j}(\vec{x}_k, t). \quad (5)$$

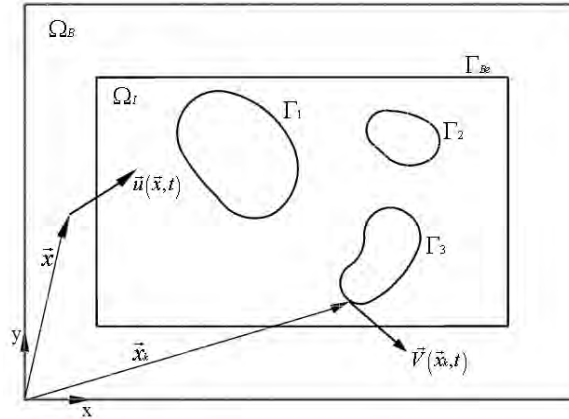


Figure 6. Schematically representation of eulerian and lagrangian domain (Mariano *et al*, 2010b).

The values of  $u_l(\vec{x}_k, t)$  and  $p(\vec{x}_k, t)$  are given by interpolation of velocities and pressure, respectively, of the Eulerian points near the immersed interface (Lima e Silva *et al.*, 2003). For Lagrangean points,  $\vec{x}_k$ , at the immersed boundary, we have:

$$F_l(\vec{x}_k, t) = \frac{u_l(\vec{x}_k, t + \Delta t) - u_l^*(\vec{x}_k, t + \Delta t) + u_l^*(\vec{x}_k, t + \Delta t) - u_l(\vec{x}_k, t)}{\Delta t} + RHS(\vec{x}_k, t), \quad (6)$$

where  $u^*$  is a temporary parameter, as defined in Wang *et al.* (2008),  $\Delta t$  is the time step and  $RHS$  are the terms of the right hand side of Eq. (5). The Eq. (6) is solved by Eqs. (7) and (8) at the same time step:

$$\frac{u_l^*(\vec{x}_k, t + \Delta t) - u_l(\vec{x}_k, t)}{\Delta t} + RHS(\vec{x}_k, t) = 0, \quad (7)$$

$$F_l(\vec{x}_k, t) = \frac{u_l(\vec{x}_k, t + \Delta t) - u_l^*(\vec{x}_k, t + \Delta t)}{\Delta t}, \quad (8)$$

where  $u_l(\vec{x}_k, t + \Delta t)$  is the immersed boundary velocity, *i.e.* the specific boundary condition, normally known.

Equation (7) is solved in the Eulerian domain in the Fourier spectral space, *i.e.* the solution of Eq. (2) with  $f_i=0$ .  $u_l^*(\vec{x}, t + \Delta t)$  is interpolated to the Lagrangean domain and became  $u_l^*(\vec{x}_k, t + \Delta t)$ . Then  $f_l(\vec{x}_k, t)$  is given by Eq. 4 for Eulerian mesh. Finally, the Eulerian velocity,  $u_l(\vec{x}, t + \Delta t)$ , is updated by Eq. 9:

$$u_l(\vec{x}, t + \Delta t) = u_l^*(\vec{x}, t + \Delta t) + \Delta t \cdot f_l(\vec{x}, t), \quad (9)$$

### 3.3 Fourier pseudospectral method

The methodology used by solving Navier-Stokes equations with IBM is the Fourier pseudospectral method (Canuto *et al.*, 2007). It consists in applied the Fourier transformed in Eqs. (2) and (3), given:

$$ik_j \hat{u}_j = 0 \quad (10)$$

$$\frac{\partial \hat{u}_l(\vec{k}, t)}{\partial t} + \nu k^2 \hat{u}_l(\vec{k}, t) = \hat{f}_l(\vec{k}, t) - ik_j \oint_{\vec{k}=\vec{r}+\vec{s}} \hat{u}_l(\vec{r}, t) \hat{u}_l(\vec{k}-\vec{r}, t) d\vec{r} \quad (11)$$

The Navier-Stokes equations, Eq. 11, are transformed to spectral space using the Discrete Fourier Transform (DFT), which is defined by Briggs and Henson (1995) and computationally performed by Fast Fourier Transform (FFT) given in Takahashi (2006). The boundary conditions are imposed by coupling IBM (Mariano *et al.*, 2010).

The convolution integral to solve the non-linear term was solved using the skew-symmetric approach (Canuto *et al.*, 2006) and the temporal evolution is performed by low dispersive and low dissipative explicit fourth order optimized Runge-Kutta (Allampalli *et al.*, 2009).

#### 4. NUMERICAL RESULTS

Figure 4 shows the physical domain,  $\Omega_{PhD}$ , (solid line), that is immersed in periodical domain,  $\Omega_{PeD}$  (dashed line). The physical domain is no periodical and is bounded by immersed boundary  $\Gamma_{PhD}$ . The periodical domain is delimited by  $\Gamma_{PeD}$  boundary. The  $\Gamma_{PhD}$  represent the “physical boundary conditions”, *e.g.*, wall boundaries, the no-slip boundary conditions in upper and bottom walls and an inlet are imposed. In the outlet  $\Gamma_{PeD}$  and  $\Gamma_{PhD}$  are coincident, where periodical boundary conditions is used.

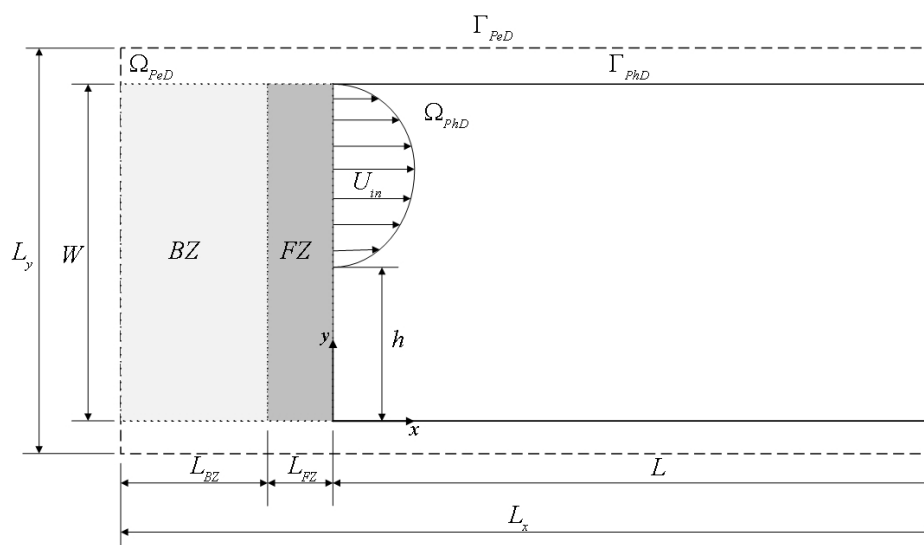


Figure 7. Domain used to Fourier pseudospectral method simulations.

The periodical boundary conditions imposed in outlet given the physical instabilities that leave the domain are reinjected in the inlet of the domain. In order to avoid that instabilities that affect the boundary conditions at  $\Gamma_{PhD}$  the buffer zone is used (zone BZ in Figure 7) in order to dissipate the vortex. The forcing zone (zone FZ in Figure 7) is used to align the streamlines at the entrance.

In forcing zone, FZ, the procedure consists enforce the inlet profile using the immersed boundary methodology. In the present paper this inlet profile is provided by Lee and Mateescu (1998) and is given by Eq. 12. This velocity profile corresponds to a developed flow in a duct which mean velocity is  $\bar{U}_{in} = 1,0 [m/s]$ .

$$U_{in}(y) = \begin{cases} 0,0 & \text{if } h < y < W \\ -2604,2 \cdot (W - y) \cdot (h - y) & \text{if } h < y < W \end{cases} \quad (12)$$

The buffer function used in the present work was proposed by Joslin *et al.*, (1991), Eq. 17. This function is used to drive the flow in a smooth way through the forcing zone:

$$BZ(x) = \phi(x)(Q - Q_t), \quad (13)$$

where  $Q_t$  is the target solution;  $Q$  is the given Navier-Stokes solution, and the stretching function,  $\phi$ , is given by Eq. 14:

$$\phi(x) = \frac{1}{2} \left[ 1 - \tanh \left( 4 - 8 \frac{x_s - x}{x_s - x_f} \right) \right], \quad (14)$$

where  $x_s$  and  $x_f$  are the start and the final positions the buffer zone, respectively.

The BZ function given in Eq. 13, is transformed to Fourier spectral domain, then, this term is projected over the plane  $\pi$  and superimposed on the estimated velocity field:

$$\hat{u}_i^*(\vec{k}, t) \leftarrow \hat{u}_i^*(\vec{k}, t) - \overline{BZ}_i(\vec{k}, t) \quad (15)$$

All simulations presented in this paper use the Runge-Kutta RK46 temporal integration, presented by Allampalli *et al.*, (2009). The time step,  $\Delta t$ , changes in agreement to CFL criterion (Courant *et al.*, 1967) where  $CFL=1,0$ . Furthermore, 1024 x 64 collocation nodes were used in  $\Omega_{ped}$  domain (Figure 7) and the other parameters to simulations are given:

$$\begin{aligned} L_x &= 2,00 \text{ m}; \\ L_y &= 2 \cdot h = 1,92 \cdot 10^{-1} \text{ m}; \\ \Delta x &= L_x/n_x = 2,00/1024 = 1,95 \cdot 10^{-3} \text{ m}; \\ \Delta y &= \Delta x = 1,95 \cdot 10^{-3} \text{ m}; \\ L_{in} &= 102 \cdot \Delta x = 2,00 \cdot 10^{-2} \text{ m}; \\ L &= L_x - L_{in} = 1,80 \text{ m}; \\ L_{FZ} &= 10 \cdot \Delta x = 1,95 \cdot 10^{-2} \text{ m}; \\ L_{BZ} &= L_{in} - L_{FZ} = 1,78 \cdot 10^{-2} \text{ m}; \\ W &= 9,60 \cdot 10^{-2} \text{ m}; \\ \rho &= 1,0 \text{ kg/m}^3; \\ CFL &= 1,0. \end{aligned}$$

The present section, the simulated flow refers to  $Re_h=400$ . The classical laminar flow with the bottom and the upper recirculation zones is visualized. These recirculations appear because of the detachment of the boundary layers. The laminar behavior for this Reynolds number is as expected.

Figure 10 presents comparisons between the results of the present work and numerical results of Gartling (1990) and the experimental results of Lee and Mateescu (1998). The streamwise velocity is shown at three points: (left)  $x/h=0,0$ , (center)  $x/h=14,0$  and (right)  $x/h=30,0$ .

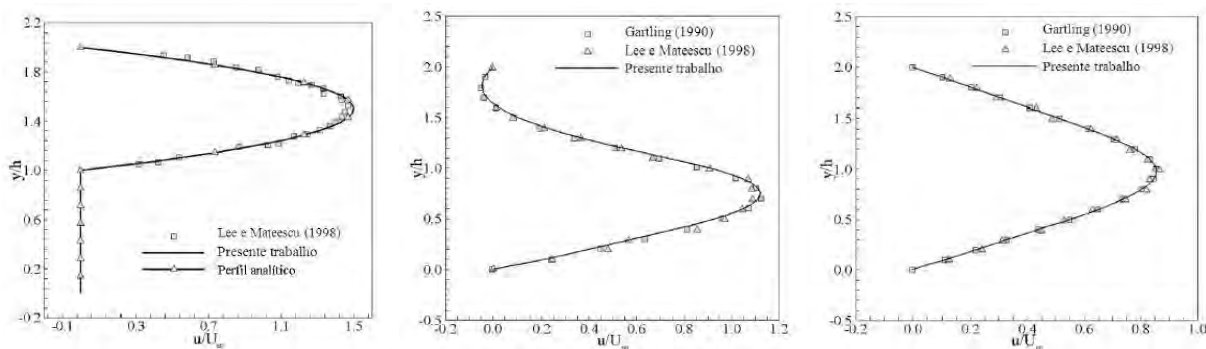


Figure 8. Flow over backward-facing step, streamwise flow in  $x/h=0,0$  (left),  $x/h=14,0$  and  $x/h=30,0$ .

At point  $x/h=0,0$  (Figure 8), very good agreement is obtained, showing that the internal boundary is well modeled by the forcing zone. At points  $x/h=14,0$  and  $x/h=30,0$ , again, very good agreement is attained with the experimental results of Lee and Mateescu (1998) and with the numerical results of Gartling (1990). This result shows that the method used to force the internal boundary condition is accurate and stable during the time evolution of the numerical experiment. It is possible to accurately reproduce the experimental measurements, regarding the numerical representation of the boundary conditions.

The simulation results to several Reynolds numbers are studied range from 100 to 3000. Figure 9 presents the vorticity fields for the backward-facing step simulations. For Reynolds numbers ranging from 100 to 400 the flow does not present any instability, as expected. For Reynolds numbers ranging from 800 to 1500, the flow becomes unstable, giving rise to Kelvin-Helmholts instabilities near the step that are transported toward the bottom wall reattachment point. Instabilities are also formed beyond the detachment point on the upper wall. These instabilities interact with each other and are transported toward the outlet of the channel. This finding is a classical result that is obtained with the proposed methodology in the present work. For Reynolds numbers ranging from 1500 to 3000, the instabilities present chaotic behavior, as expected for higher Reynolds numbers.

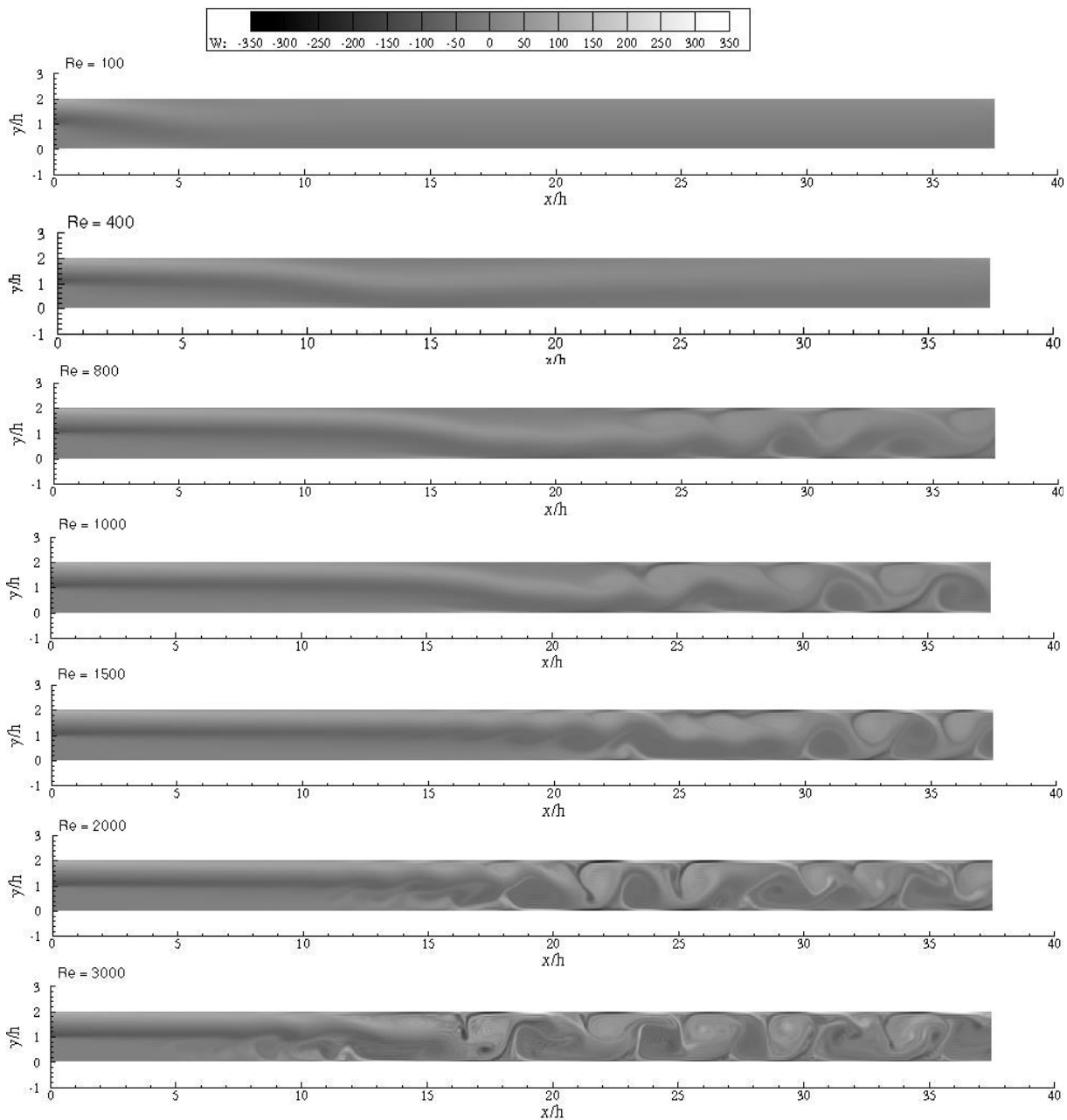


Figure 9. Results of the simulations to different Reynolds numbers.

By comparing the pictures of experiment of the Figure 4 and numerical results of Figure 9 is possible to determine the transitional range from laminar to turbulent flow. Specifically, to backward-facing step with aspect ratio equal two the transitional range begin at  $Re_h=500$  and go to 1500. Reynolds numbers higher than 1500 the flows are already turbulent. The multiplicity of turbulence scales can be observed, into main recirculation arise several small eddies, and, into channel the large eddies, are formed.

Table 1 shows the reattachment point at the bottom wall ( $x_r/h$ ), for several Reynolds number values and a comparison with the experimental results of Lee and Mateescu (1998). There is good agreement for Reynolds numbers smaller than 400. For higher values of this parameter, the error increases as expected for two-dimensional simulations, as was also reported in Armaly *et al.*, (1993).

Table 1. Comparison of mean position of reattachment point,  $x_r=h$ , for different Reynolds number.

$Re_h$	Lee and Mateescu (1998)	Present work
100	-	5.2
400	13.0	12.1
500	15.1	13.4
800	13.2	16.7
1000	12.5	18.8
1500	10,5	25.6
2000	-	19.8
2500	-	16.6
3000	-	15.1

## 5. CONCLUSIONS

In the present article the flows over backward-facing step are studied numerically by Fourier pseudospectral method and visualized by experimental setup. The both procedures show that the transitional range from laminar to turbulent flow occurs between  $500 < Re_h < 1500$ . The experimental of the present paper is a simple procedure, nevertheless allows visualized the flow and established the transitional range, when the flow start the generate Kelvin-Helmoltz instabilities.

The differences presented in Tab. 1 can be explained due the comparison of the experimental results (Lee and Mateescu, 1998), which are three-dimensional flows, and the two-dimensional numerical results. When the flow is in transitional range the turbulent effects appears and the flow requires the spanwise direction, because the nature dissipate and diffusive of turbulence.

## 6. ACKNOWLEDGEMENTS

The authors thank the School of Engineering Electrical, Mechanical and of Computational (EMC) of the University Federal of Goiás (UFG), FAPEG, CAPES, CNPq and Petrobrás for financial support.

## 7. REFERENCES

- Allampalli, V., Hixon, R., Nallasamy, M., Sawyer, S., 2009, "High-accuracy large-step explicit Runge-Kutta (HALE-RK) schemes for computational aeroacoustics. *Journal of Computational Physics*, Vol. 228, pp. 3837-3850.
- Armaly, B.F., Durst, F., Pereira, J.C.F., and Schonung, B. 1983, "Experimental and theoretical investigation of backward-facing step flow", *Journal of Fluid Mechanics*, Vol. 127, pp. 473-496.
- Canuto, C., Hussaini, M.Y., Quarteroni, A. and Zang, T.A., 2007, "Spectral methods: evolution to complex geometries and applications to fluid dynamics", Ed: Springer-Verlag, New York, United States, 596p.
- Enriquez-Remigio, S. and Silveira-Neto, A., 2007, "A new modeling of fluid-structure interaction problems through immersed boundary method/virtual physical model (IBM/VPM)", *Proceedings of the 19th Brazilian Congress of Mechanical Engineering*, Vol.1, pp. 1-10.
- Ferziger, J.H. and Peric, M., 2002. "Computational Methods for Fluid Dynamics". Ed: Springer Verlag, 3rd edition, Berlin, Germany.
- Fornberg, B., 1980. "A numerical study of steady viscous flow past a circular cylinder". *Journal of Fluid Mechanics*, Vol. 98, No. 4, pp. 819-855.
- Gartling, D.K., 1990. "A test problem for outflow boundary conditions - flow over a backward-facing step". *International Journal of Numerical Methods in Fluids*, Vol. 11, pp. 953-967.
- Goldstein, D., Handler, R. and Sirovich, L., 1993. "Modeling a no-slip flow with an external force field". *Journal Computational Physics*, Vol. 105, pp. 354-366.
- Griffith, B.E. and Peskin, C.S., 2005, "On the order of accuracy of the immersed boundary method: higher order convergence rates for sufficiently smooth problems", *Journal Computational Physics*, Vol. 208, pp. 75-105.
- Le, H., Moin, P. and Kim, J., 1997. "Direct numerical simulation of turbulent flow over a backward-facing step". *Journal of Fluids Mechanics*, Vol. 330, pp. 349-374.
- Lee, T., and Mateescu, D., 1998. "Experimental and numerical investigation of 2-D backward-facing step flow". *Journal of Fluids and Structures*, Vol. 12, pp. 703-716.
- Mariano, F.P., Moreira, L.Q. and Silveira Neto, A., 2010a, "Mathematical Modeling of non-periodic flows using Fourier pseudo-spectral and immersed boundary methods", *Proceedings of the 5th European Conference on Computational Fluid Dynamics*, Vol.1, Lisbon, Portugal, pp. 1-17.
- Mariano, F.P., Moreira, L.Q., Silveira-Neto, A., Silva, C.B. da, Pereira, J.C.F., 2010b, "A new incompressible Navier-Stokes solver combining Fourier pseudo-spectral and immersed boundary method. *Computer Modeling in Engineering Science*, v. 59, p. 181-216.

W.A. Mazan Júnior, C.A.A. Vilela and F.P. Mariano  
Experimental and Computational Simulations of the Flow over Backward Facing Step

- Park, J., Kwon, K. and Choi, H., 1998. "Numerical solutions of flow past a circular cylinder at Reynolds numbers up to 160". *KSME International Journal*, Vol. 12, No. 6, pp. 1200–1205.
- Patankar, S.V., 1980. "Numerical Heat Transfer and Fluid Flow". Ed: McGraw-Hill, New York.
- Peskin, C.S., 2002, "The immersed boundary method", *Acta Numerica*, Vol.11, pp. 479–517.
- Sahin, M., and Owens, R.G., 2004. "A numerical investigation of wall effects up to high blockage ratios on two-dimensional flow past a confined circular cylinder". *Physics of Fluid*, Vol. 16, No. 5.
- Wang Z., Fan J. and Luo, K., 2008, "Combined multi-direct forcing and immersed boundary method for simulating flows with moving particles", *International Journal of Multiphase Flow*, Vol.34, pp. 283-302.
- Ye, T., Mittal, R., Udaykumar, H.S. and Shyy, W., 1999. "An accurate cartesian grid method for viscous incompressible flows with complex immersed boundaries". *Journal of Computational Physics*, Vol. 156, pp. 209–246.

## 8. RESPONSIBILITY NOTICE

The authors are the only responsible for the printed material included in this paper.